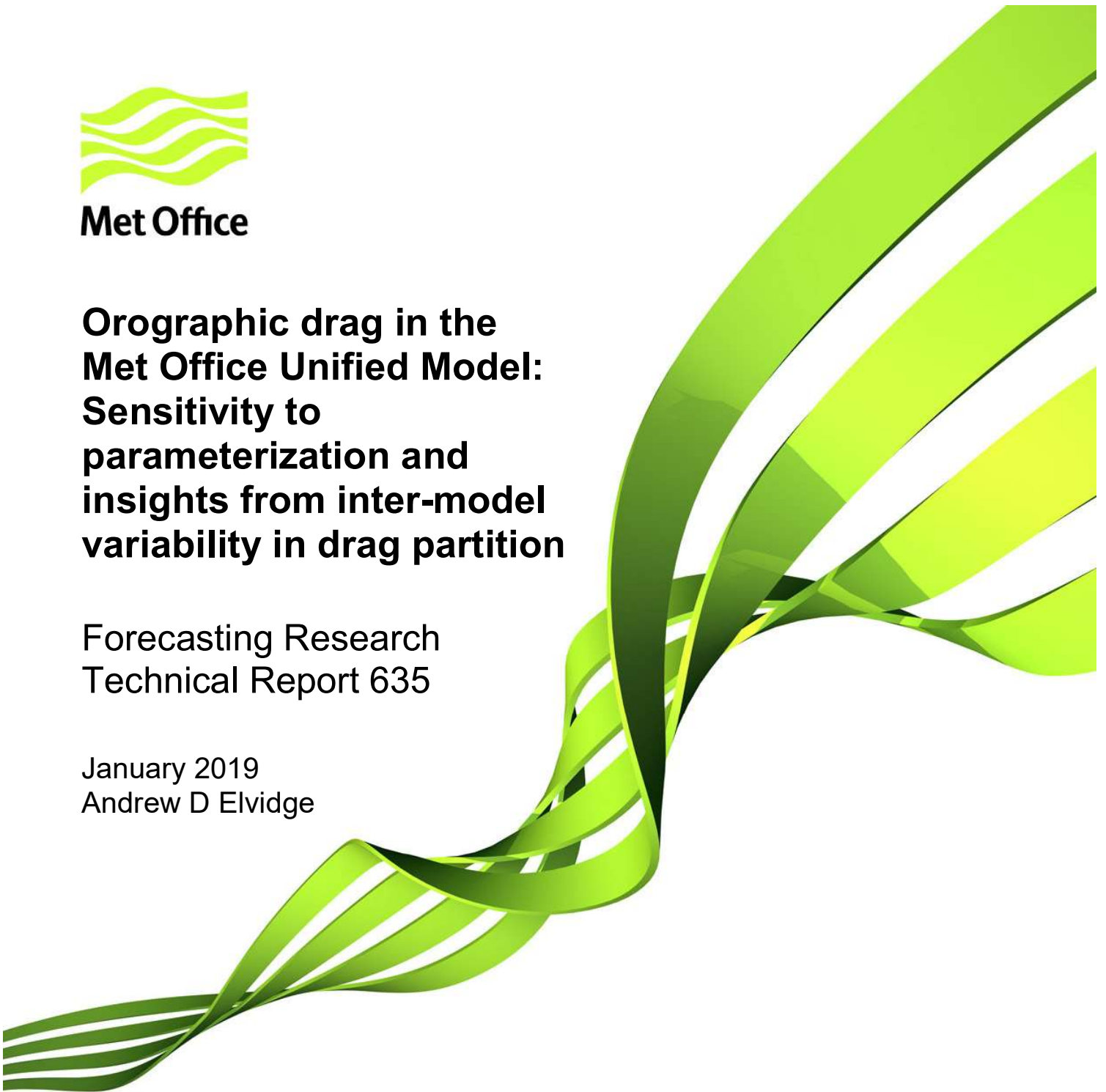**Orographic drag in the Met Office Unified Model: Sensitivity to parameterization and insights from inter-model variability in drag partition**

Forecasting Research
Technical Report 635

January 2019
Andrew D Elvidge

Abstract

Global model experiments investigating the sensitivity of MetUM performance at both NWP and climate time-scales to individual changes in orographic drag parameterization indicate that forecast improvements may be possible via the retuning of orographic drag scheme parameters, reassuringly towards more physically realistic values. The experiments reveal considerable model sensitivity to drag parameterization configuration. The most beneficial changes are found to arrive via decreases in the low level drag associated with orographic flow blocking and an increase in the higher-altitude drag associated with gravity wave breaking. The former has the effect of reducing high latitude high pressure biases in the MetUM, whilst the latter improves in particular temperature distribution, and to a lesser extent circulation, in the stratosphere. These tendencies in stress components may be brought about via changes to each of the five tuneable orographic drag scheme parameters. For four of the five parameters, these changes yield values which are closer to those recommended in the literature (whilst the fifth parameter, being poorly constrained, is relatively flexibly tuneable).

In a month-long global model comparison between the MetUM and ECMWF IFS, considerable differences in drag partition are identified, highlighting the considerable uncertainty in the representation of orographic drag that remains. This disparity is linked to differences in the diurnal and spatial variability in surface stress over high mountain ranges. The MetUM displays marginally higher amplitude diurnal variability – arguably the opposite of that which would be intuitively expected. The beneficial tendencies in drag components found in the MetUM sensitivity experiments – an increase in gravity wave drag and a decrease in flow blocking drag (plus an ensuing compensating increase in boundary layer drag) – would bring the MetUM into closer agreement with the partition of drag components seen in the IFS.

1   Background

Surface momentum exchange plays a governing role in the atmosphere's general circulation. It explains the surface wind pattern of tropical easterlies and mid-latitude westerlies whilst, higher in the atmosphere, the location of the subtropical and mid-latitude westerly jets are dependent on it (Stephenson, 1994; Robinson, 1997; Chen et al., 2007). The drag exerted by mountains on the atmosphere acts across a wide range of scales and is the result of various mechanisms, often sub-grid scale in operational forecast products. The importance of mountain wave drag on the large-scale momentum budget has been acknowledged since the infancy of NWP; its parameterization found to be necessary in counteracting the mid-latitude westerly wind bias present in the earliest models (e.g. Palmer et al., 1986; McFarlane, 1987). Such waves transport momentum vertically in the atmosphere, exerting a drag force on the mean flow upon breaking at some height above the orography. At lower levels in the atmosphere, mountains exert a blocking drag force on the flow below mountain-top level, forcing flow around the mountain and causing flow separation at its flanks (Lott and Miller, 1997). The integration of flow blocking into orographic drag schemes since the turn of the century has brought marked improvements in NWP and climate model performance (Scinocca and McFarlane 2000; Zadra et al., 2003; Sandu et al., 2013; Pithan et al., 2015). Finally, at smaller orographic length scales,

turbulence generated in the lee of undulating terrain exerts a form drag force in the boundary layer (Wood and Mason, 1993).

Despite recognition of its importance for weather forecasting and climate prediction, the representation of drag processes associated with surface stress is a major source of uncertainty in general circulation models (GCMs); their ability to accurately conserve angular momentum and represent momentum exchanges being poorly understood. The parameterization schemes used to represent orographic drag are poorly constrained and in any case tend to be tuned to optimize model skill rather than to accurately represent physical processes. Early output from the Working Group on Numerical Experimentation (WGNE) drag project has demonstrated considerable inter-model variability in both total sub-grid surface stress and the proportional allocation of stress into its various contributions over land (with zonally averaged total surface stresses differing by as much as 20%), in particular over orography (Zadra, 2015; Sandu et al., 2016). Sandu et al. (2016) has shown that the extent of such variability is significant to Northern Hemisphere winter circulation at both daily and seasonal time scales.

Sandu et al. (2016) ran two experiments with the Integrated Forecasting System (IFS) with parameter changes in each of two different drag schemes (orographic form drag and flow blocking). These changes led to similar increases in zonally averaged total surface stress, yet the response in surface pressure was quite different. They hypothesised this could be a result of differences in the spatial distribution and the diurnal cycle of the stress. The work presented in Section 3 follows on from the study of Sandu et al. by investigating spatial and diurnal variability in the partition of orographic stress between two models: the Met Office Unified Model (MetUM) and the Integrated Forecast System (IFS) of the European Centre for Medium-Range Weather Forecasts (ECMWF).

In their handling of subgrid orographic stresses, the MetUM and IFS adopt generally similar conceptual approaches (see Section 2 for more details). These schemes include a number of tunable parameters. Using high resolution MetUM modelling, Vosper (2015) and Vosper et al. (2016) found that the parameter settings used in the current operational global model were not optimal for the mountainous islands of South Georgia or New Zealand individually, and that optimal settings varied between these regions. The regional sensitivity of drag in the MetUM to parameter settings together with the significant inter-model variability in drag representation points towards scope for improvement in the representation of drag; the simplest means of doing so being simple parameter settings. In Section 4, a series of MetUM experiments are conducted to test both NWP and climate forecast sensitivity to one-at-a-time changes in drag parameter settings and other alterations to the schemes responsible for the representation of orographic drag.

2   The representation of subgrid scale orographic stress in weather and climate modelling

Owing to the various different mechanisms responsible for drag in the atmosphere, models commonly represent subgrid stress via several different algorithms, often residing in different physics regimes. In both the MetUM and IFS, unresolved stress due to surface features of horizontal scales less than ~5 km are dealt with in the

boundary layer scheme, while the subgrid scale orography (SSO) scheme represents stress associated with horizontal scales between 5 km and the model resolution.

For the parameterization of SSO drag, both the MetUM and IFS employ the scheme of Lott and Miller (1997), which is based on two separate conceptual models: bluff-body dynamics for the low-level drag associated with flow blocking and linear gravity-wave theory for the mountain-wave drag. The partition of stress amongst these two contributions is dependent on the flow regime, as described by the local depth-averaged Froude number (*Fr*). In subcritical flow regimes (where *Fr* is smaller than a fixed critical value), some air is assumed to be blocked and to flow around the mountain barrier, resulting in flow separation at the flanks and a low-level drag force exerted on the flow.

Above the blocked layer, the air is assumed to rise over the remainder of the mountain (the *cut-off* mountain), resulting in the generation of hydrostatic gravity waves. The expression for the parameterized mountain-wave momentum flux is based on the linear solution for elliptical mountains derived by Phillips (1984). The total parameterized orographic drag at the surface is the sum of the blocking and gravity wave drag. However, whilst the flow blocking drag is applied below the cut-off mountain height, gravity wave drag is only deposited upon wave breaking at heights where the non-dimensional local wave amplitude surpasses a set critical value. An overview of the current operational version of the MetUM SSO scheme (the 5A scheme) is provided in the Appendix of Vosper (2015), and that of the IFS in Chapter 4 of ECMWF (2013).

The parameterization of turbulent orographic form drag varies between the two models. In the IFS it is handled explicitly in terms of a slope parameter for sinusoidal hills (Beljaars, 2004), whereas in the MetUM it is currently represented by an effective roughness length (e.g. Wood and Mason, 1993), though a new distributed scheme similar to that of the IFS is pending adoption.

3   Diurnal and spatial variability in surface stress over orography in the Met Office UM and ECMWF IFS

3.1   Models and Methods

A series of simulations have been run using the MetUM and IFS at ~16 km horizontal resolution (TL1279 in the former, N768 in the latter) over a single Northern Hemispheric winter month (December 2015), with each model run initiated daily at 00 UTC and running for a duration of 24 hours. Output fields are time-averaged with a sampling period equal to the model time step and output 6-hourly. The total surface stress is made up of boundary layer (BL) and subgrid orography (SSO) components. In the IFS, the BL stress contribution is further segmented into turbulent orographic form drag (TOFD; representing subgrid orography elements with horizontal scales less than 5 km) and TURB (non-orographic) components. In the MetUM, TOFD stress is represented by artificially enhancing the surface roughness length over orography, and as such is implicit within the BL turbulence scheme (thus TOFD and TURB are non-separable in the MetUM). As outlined in Section 2, the partition of SSO stress into gravity wave (GW) and flow blocking

(BLOCK) components is in each grid box dependent on the local flow regime, which is governed by the subgrid mountain height, the wind speed and static stability (as described by the Froude number).

Three mountain regions provide the focus for this study: the Himalayas, the Rockies and the Andes – three of the most productive source regions for orographic drag (Figure 1; the latter also evident in the peak in Figure 2 at a latitude of ~45°S).
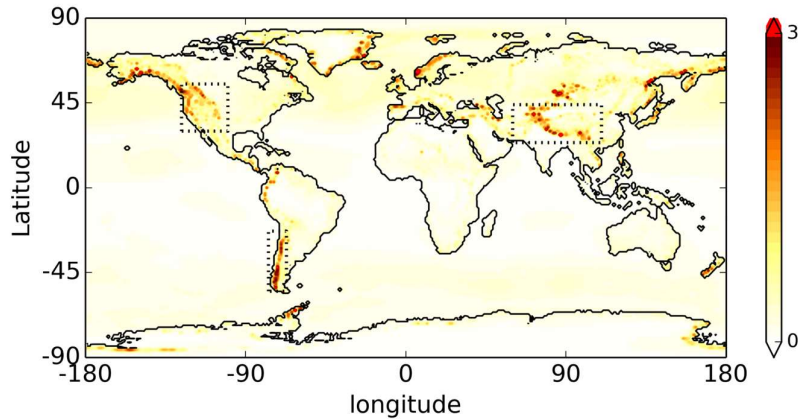

Figure 1: Total parameterized surface stress magnitude from the MetUM averaged over the month of December 2015. Hatched boxes show the locations of the three focus regions, coinciding with high stress magnitudes.

3.2   Drag partitioning and diurnal and spatial variability in surface stresses

Figure 2 shows the zonally averaged global parameterized surface stress magnitudes over land for both models, averaged over the month. There is generally good agreement between the two models in the total surface stress; however the MetUM parameterizes greater total surface stresses (by ~10 %), and the partition of this stress into its constituent components differs greatly. Across all latitudes, the MetUM assigns more of the surface stress to the SSO scheme (230 % greater globally, as a result of a 240 % greater BLOCK stress and a 180 % greater GW stress), whilst the IFS assigns more to the BL scheme (7 % greater globally; note that the global sum of BL stresses is greater than that of SSO stresses by a factor of ~3 and ~12 in the MetUM and IFS respectively). In Figure 3, the diurnal cycle in the mean wind speed and Brunt-Väisälä frequency used by the MetUM SSO scheme and of the surface stresses for each mountain range is illustrated. Unsurprisingly, the difference between the two models in stress partitioning between the BL and SSO schemes is particularly apparent for these regions of high parameterized orographic stresses. Furthermore, over all three mountain ranges, the MetUM exhibits consistently and markedly greater (generally by ~15 %) total surface stresses.

In all three regions and in both models the surface stresses exhibit a clear diurnal cycle, dominated by the variability in BL stress (Figure 3). Peak stresses occur during the daytime, coinciding with lower static stabilities and stronger wind speeds. Diurnal variation in the SSO drag components is theoretically more complex owing to the non-linear dependence of each of the components on the mean flow speed, static stability and terrain properties. In the present cases there is consistently a

4

relatively weak diurnal variability in the SSO surface stress, which is opposite in sign to that of the BL stress, i.e. peaking during the night. This may be explained by reduced winds and increased static stabilities leading to a general decrease in Froude number and consequently enhanced flow blocking, which dominates over variability in the already small GW stress contribution. Given the larger BL contribution (with a strong daytime peak) in the IFS and the larger SSO contribution (with a weak nighttime peak) in the MetUM, it might be expected that the IFS would exhibit a more pronounced diurnal cycle in surfaces stresses. In fact the opposite is true for all three regions, though only marginally so (see the "IFS - MetUM" difference panels in Figure 3).
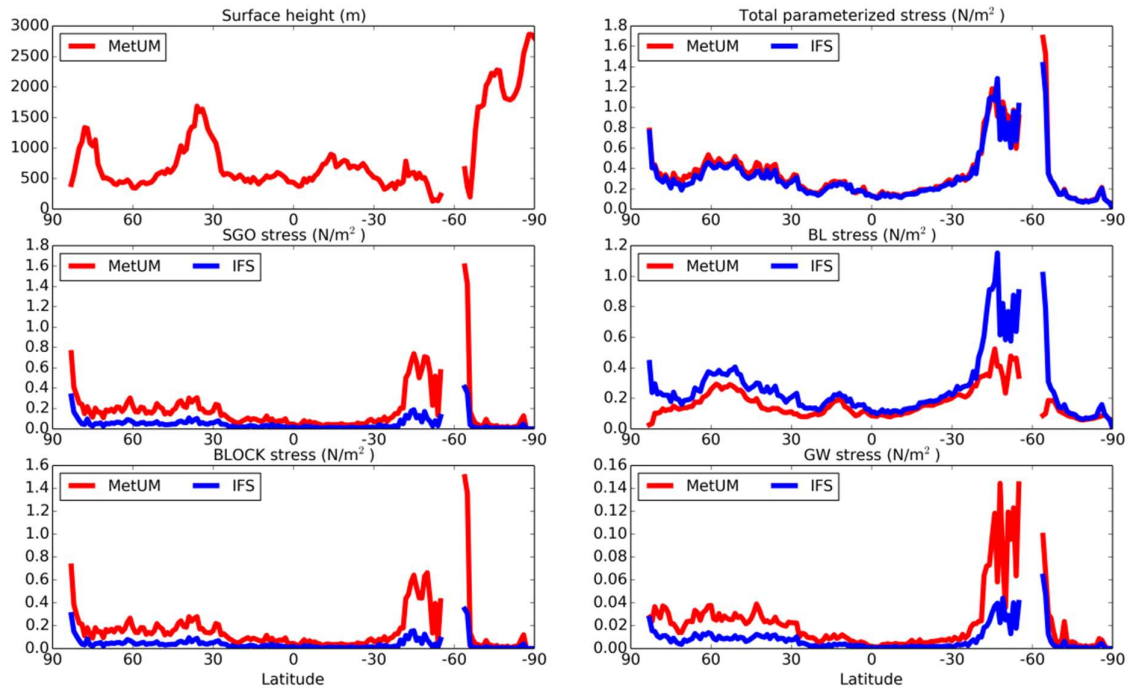

Figure 2: Zonally averaged surface height (top left), total parameterized surface stress magnitude (top right) and surface stress magnitude components (the four panels below) over land from the MetUM and IFS, averaged over the month of December 2015.
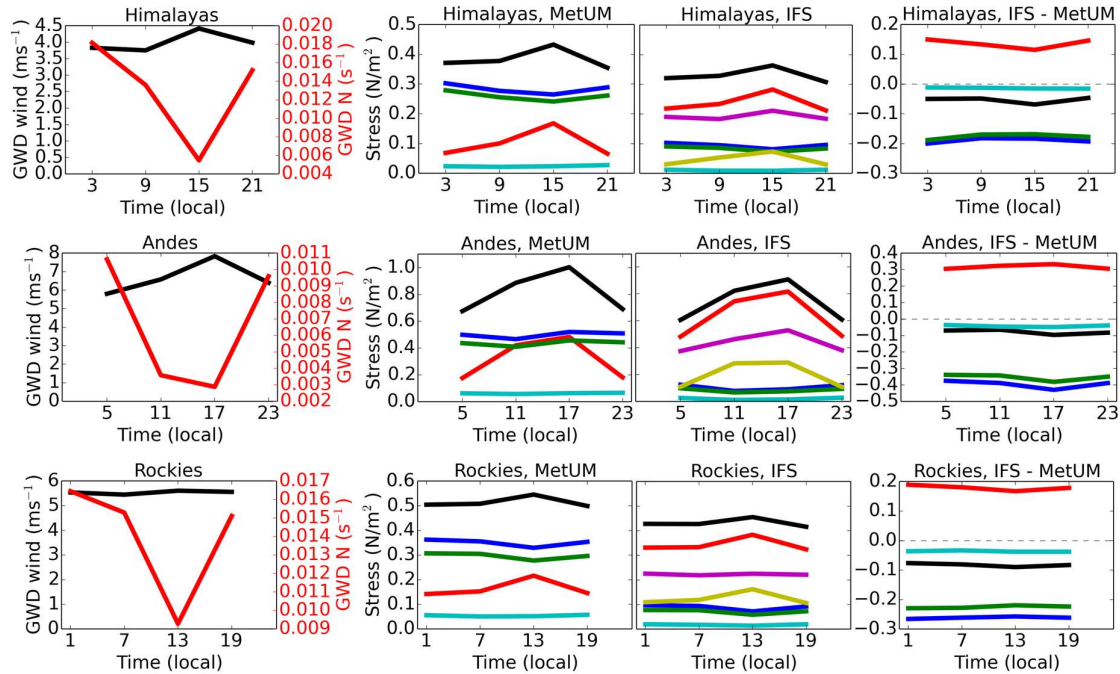
Figure 3: December 2015 diurnal cycles of the **depth-averaged wind speed** and **Brunt-Väisälä frequency** used by the MetUM SSO scheme (column 1), surface stress magnitudes in the MetUM (column 2) and IFS (column 3) and the difference (IFS - MetUM; column 4). The stress components are **TOTAL**, **BL**, **SSO**, **BLOCK**, **GW**, **TOFD**, **TURB**. Each time (x axis) refers to the mid-point of the six-hourly mean values.

Over the Himalayas, despite the difference in partitioning, in both the MetUM and IFS the greatest surface stresses are found along the steep south and west slopes, which are windward with respect to the prevailing (Southwesterly) flow (figure 4). Likewise, in the Rockies and Andes regions the locations of peak BL stresses in the IFS largely coincide with peak SSO stresses in the MetUM (not shown).

Figure 5 shows mean differences in surface stress magnitudes between day and night in both models over the Himalayas. The greater diurnal variability in the MetUM is apparent, not only in the BL stress but also in the SSO stress components. Over the highest ground there is a distinct daytime positive bias in wind speed, associated with enhanced BL stress. There is also a handover between the BL and SSO stress contributions between day and night in the MetUM. This pattern is also seen in the IFS, though to a lesser degree.

The spatial variability evident in the SSO stress components in Figure 5 highlights the complex dependence of these stresses on atmospheric conditions and terrain properties. Stronger daytime winds and weaker stabilities over the Himalayas are associated with greater daytime SSO stresses over the steep south westerly slopes, yet weaker daytime SSO stresses over the Tibetan plateau where slopes are gentler and subgrid mountain heights smaller.
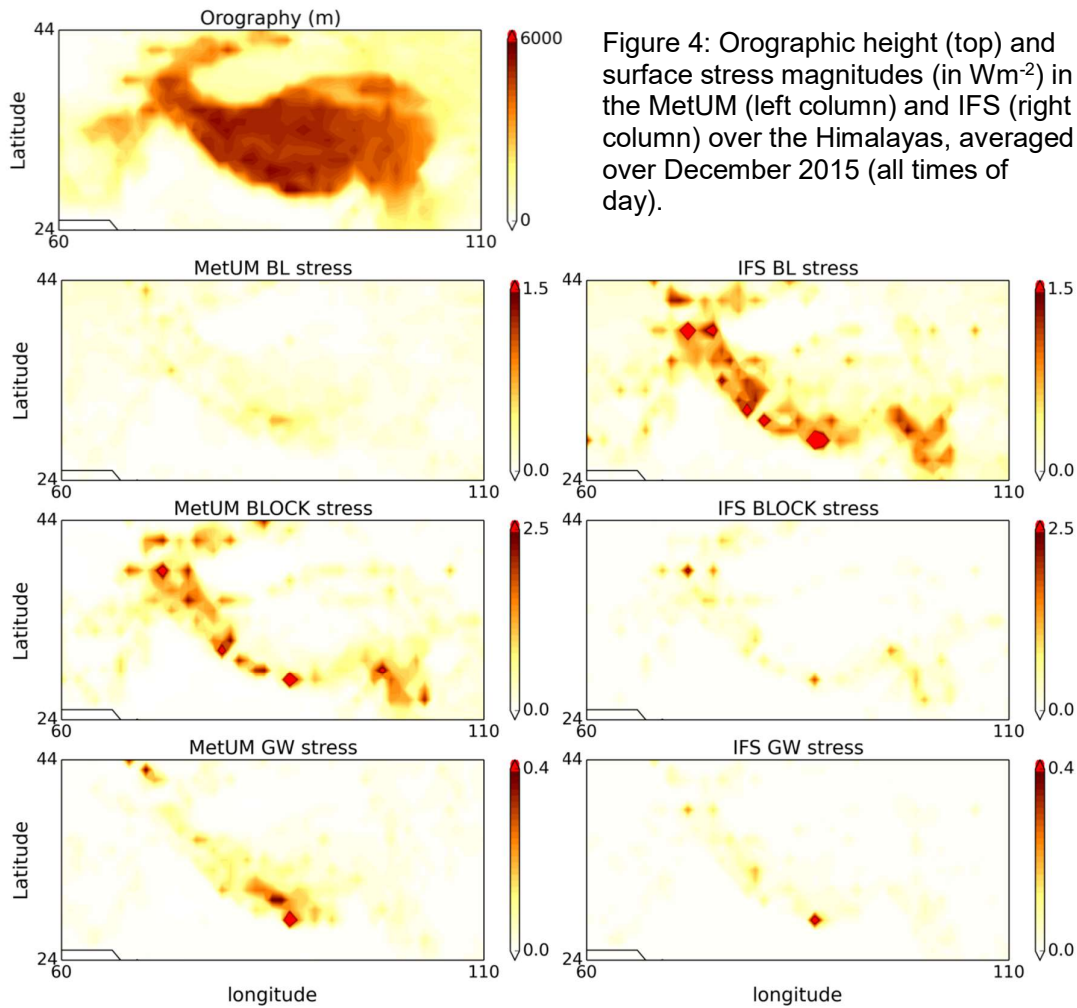
Figure 4: Orographic height (top) and surface stress magnitudes (in Wm^{-2}) in the MetUM (left column) and IFS (right column) over the Himalayas, averaged over December 2015 (all times of day).

3.3 Discussion

Whilst the MetUM and IFS models (at similar resolutions) show generally good agreement in the zonally-averaged total global orographic surface stress, total surface stresses in the MetUM are on the whole greater (by ~10 %) than in IFS. This may be explained by differences in the processing of orography fields used by each model. For reasons of numerical stability, smoothing is applied to the mean orography used by both models, and the degree of smoothing is significantly greater in the MetUM than in the IFS (Irina Sandu, personal communication, 2016). This is likely to result in greater resolved stresses and consequently weaker parameterized stresses in the IFS. However, differences in parameter settings are also likely to be pertinent.
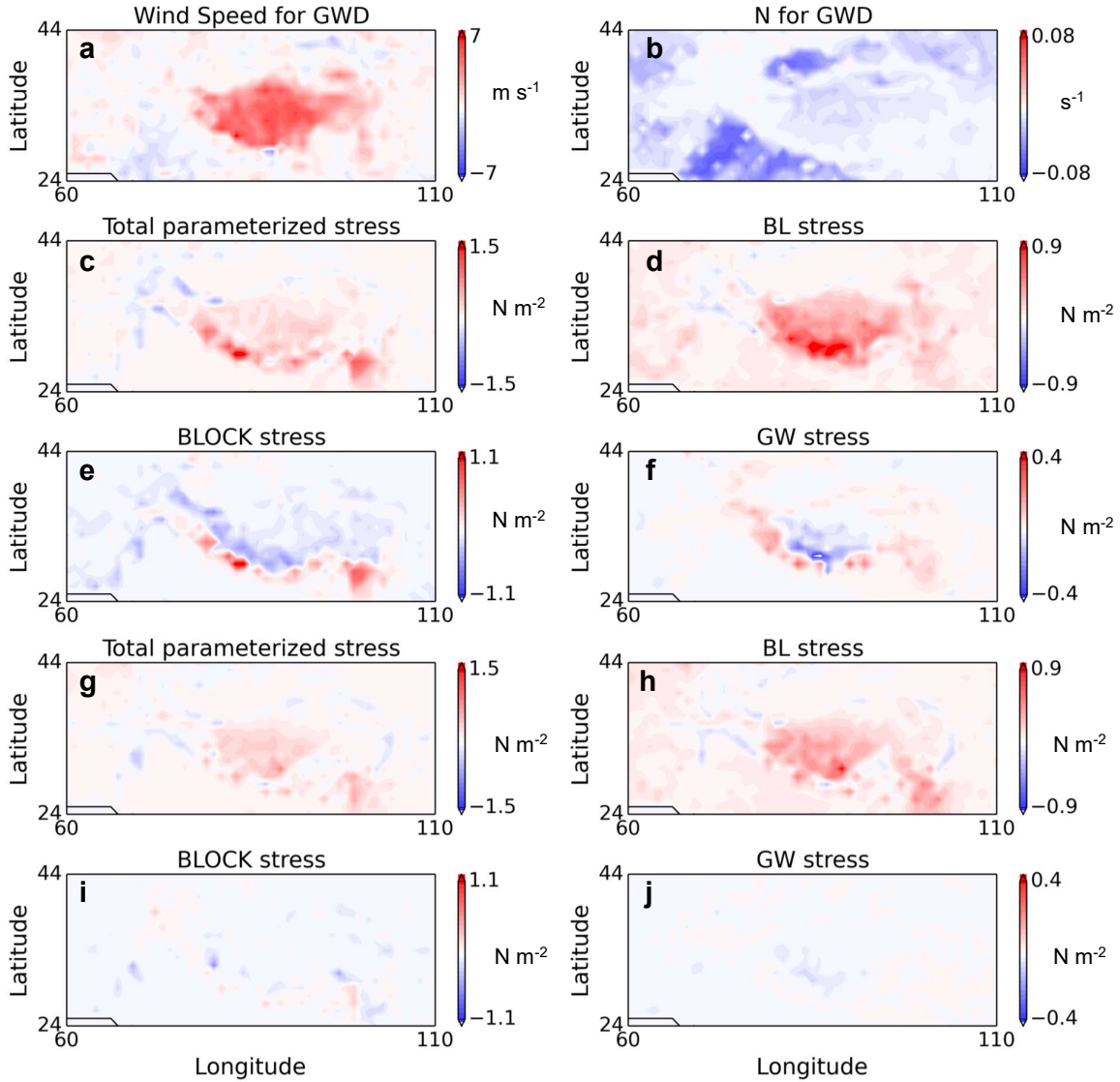
Figure 5: Mean daytime-nighttime difference in the (a,b) depth-averaged wind speed and Brunt-Väisälä frequency used by the MetUM SSO scheme; surface stress magnitudes over the Himalayas in (c-f) the MetUM; and in (g-j) the IFS. For each diagnostic, mean nighttime (00 to 06 local time) values have been subtracted from mean daytime (12 to 18 local time) values.

Another key difference in drag representation between the two models is the partition of stresses into their constituent components. In the MetUM the SSO scheme contributions are over twice as great; whilst in the IFS the BL scheme contribution is greater. This inter-model variation highlights the existing uncertainty in the representation of orographic drag. The variation in the drag components gives rise to variations in the spatial distribution of stress – the MetUM simulation exhibiting markedly greater (generally by ~15 %) total surface stresses over high mountain ranges. Given that both models use similar SSO parameterization schemes based on the scheme provide by Lott and Miller (1997), the differences in partitioning are likely as a result of differences in parameter settings and/or the generation of the SSO orography ancillary data. Indeed, a much lower drag coefficient (C_d; as defined

later in Section 4) is used in the flow blocking scheme of the operational global IFS (where $C_d = 2$) compared to that of the MetUM (where $C_d = 4$). Furthermore, although the models handle TOFD in different ways, in the MetUM the drag coefficient used in its effective roughness approach is smaller than that recommended from a physical perspective by Mason (1987) by half.

The sensitivity of BL and SSO drag to static stability is opposite in sign – i.e. in higher stabilities, turbulent BL stresses will decrease whilst SSO stresses will increase, primarily through greater BLOC stresses (GW stresses will increase only where winds are sufficiently strong such that the mountain flow regime is supercritical, i.e. the local depth-averaged Froude number is greater than the critical Froude number, F_c; discussed further in Section 4). In both models, the diurnal cycle is largely governed by the BL contribution, which is greater during the day as a result of stronger winds and weaker static stability. There is an opposite, weaker and more spatially variable diurnal cycle in the SSO stresses, with lower stresses during the day, due to greater Froude numbers reducing flow blocking and weaker static stabilities limiting the parameterized momentum transport by mountain waves. Despite the tendency in the MetUM toward greater SSO stresses and weaker BL stresses, the diurnal variability in total stress spatially averaged over a mountain range is in fact marginally greater in the MetUM due to a greater diurnal variability in BL stresses. Within each mountain range, the diurnal variation in SSO stresses is spatially variable, both in amplitude and sign. Whilst the sign of this variability is largely consistent across models, the amplitude is generally greater in the MetUM.

4   NWP and climate model sensitivity to the parameterization of orographic drag in the MetUM

4.1   Methodology

The MetUM has been employed in the form of Atmospheric Model Intercomparison Project (AMIP) style atmosphere-only long-range climate integrations and short-range NWP "case study" integrations to investigate the sensitivity of model performance to the parameterization of orographic drag. Both modelling approaches employ the most recent Global Atmosphere 7.0 (GA 7.0) science configuration. For the AMIP-style integrations, the model is run in hindcast mode from September 1988 to December 2008. For each integration, the first four months are discarded to eliminate spin-up effects, leaving 20 years of data. For each NWP integration, twenty four case studies between 2011 and 2014 are hindcast using 5-day n320 MetUM simulations. The resulting integrated data covers both summer and winter seasons, and day and night times of day, equally.

For each climate and NWP integration model settings responsible for orographic drag representation are adjusted. The resulting hindcasts are compared with ECMWF ERA-Interim reanalysis data, affording investigation into the sensitivity of MetUM drag representation and performance at both short and long time-scales to individual changes in drag parameterization. For the assessment of model performance, Northern Hemisphere (NH) winter (December, January and February) conditions are focussed upon. Each MetUM experiment involves a drag parameter or configuration modification in either the SSO or BL scheme. Where parameter changes are concerned, the purpose of these sensitivity experiments is to get a

handle on how each parameter affects model performance, rather than to pinpoint an optimal configuration. Accordingly, for each parameter a *high* and *low* value is trialled. These values are typically, though not always, within the range deemed in the literature to be physically reasonable.

For reference, Figures 6 and 7 show zonally-averaged surface stresses and the vertical cross section of zonally-averaged gravity wave stress respectively, all time-averaged from the NWP case study integration for the *Control* experiment, where drag parameterization is configured in accordance with the operational global model. Note that the resolved stress field is output directly from the model as the integrated surface pressure drag.
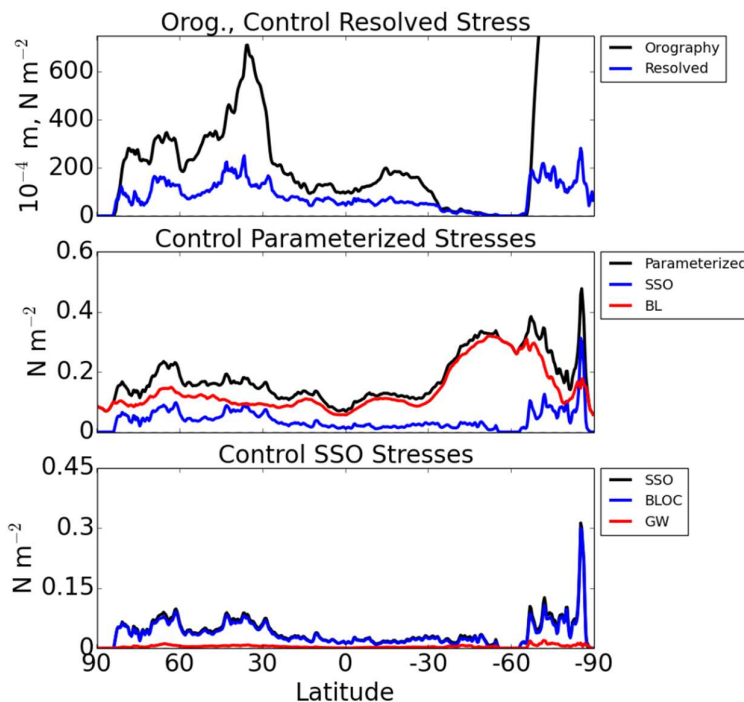

Figure 6. Zonally averaged orography and global surface stress magnitudes time-averaged over the NWP integration using operational (*Control*) settings at a lead time of 24 hours.

In Figure 6 the domination of BLOC surface stresses over GW stresses is notable. However, whilst flow blocking only occurs at low level beneath mountain top height, the global distribution of gravity wave drag is not vertically confined, often depositing momentum on the mean flow at heights well up into the stratosphere (Figure 7). Consequently, the impact of each SSO component on model performance is markedly different and it is not pertinent to compare their surface magnitudes. Figure 7 shows the vertical distribution of parameterized GW stresses across latitude bands; the band incorporating the Southern reaches of the Andes Mountains (~40-50 °S) being the most potent as a source of parameterized GW drag, owing to strong circumpolar westerlies and steep orography. GW stresses are seen to extend well into the stratosphere.

In Section 4.2, the sensitivity experiment results are presented; set out by listing in turn each change in drag configuration. The significance and context of each modification is discussed, followed by discussion on the resultant NWP and climate impacts.
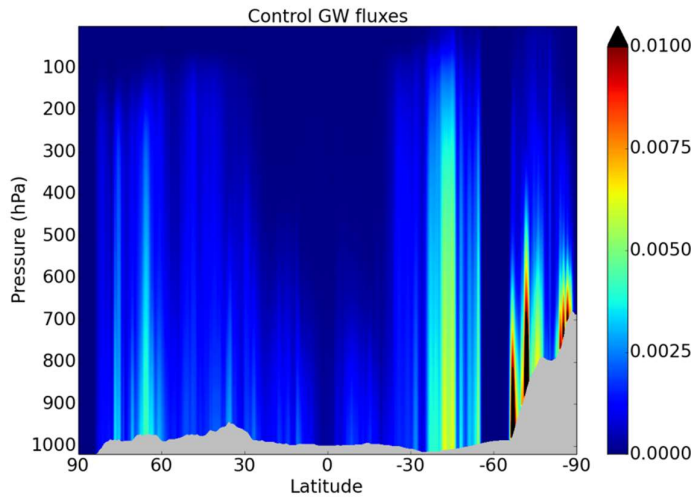
10

Figure 7. Vertical cross section of zonally-averaged orographic gravity wave stress (N m^{-2}), time-averaged over the NWP integration using operational (*Control*) settings at a lead time of 24 hours.

4.2   Sensitivity trial descriptions and results

4.2.1   Subgrid orography height coefficient, n_σ

This scaling factor is applied to the standard deviation of the subgrid orography, σ, to give a representative subgrid mountain height, $h = n_\sigma \sigma$, used by the MetUM's orographic drag scheme. Consequently, n_σ directly modulates both the total parameterized drag and, via the Froude number, the partition of drag into flow blocking and gravity wave breaking components. In the operational global model n_σ is set to 2.5, however it is a poorly constrained parameter. In Vosper (2015) and Vosper et al. (2016), high resolution MetUM simulations over South Georgia and New Zealand demonstrate that whilst the value of 2.5 is appropriate over New Zealand, a greater value (~5) is required over South Georgia due the island's simpler form (i.e. with less power in the smaller orographic length scales). To test the sensitivity of the model to this parameter, experiments are conducted with n_σ set to a *low* value of 1.5, and a *high* value of 5.

The modifications in n_σ have a marked affect on total surface stress magnitudes in the NWP experiments, primarily via changes in the BLOC stress component (Figure 8). The changes in total SSO stress, correlated with the n_σ alterations, are associated with an opposite-sign change in BL stresses. Since n_σ does not appear in the formulation of BL stresses, this is a compensating effect related to changes in surface winds; i.e. an increase (decrease) in SSO stresses leading to a decrease (increase) in surface winds, and consequently a decrease (increase) in BL stresses. The *low* n_σ setting results in zonally averaged stresses being dominated by BL contributions across most latitude bands, whilst the *high* n_σ setting leads to SSO stresses exceeding BL stresses across the more mountainous latitude bands. Although not readily apparent in Figure 8, the GW stress tendency due to changes in n_σ has the same sign as the BLOC tendency. This is shown in Figure 9 for *low* n_σ. A decrease in n_σ brings about a general increase in Froude number, both directly via reduced subgrid mountain heights and indirectly via strengthened low level winds as a result of the reduced combined low level drag from BLOC and BL components. This promotes a transfer of stresses from BLOC to GW components. However, decreased n_σ also limits the cut-off mountain height and consequently the

11

momentum carried by parameterized gravity waves. It would appear that, on the whole, the effect of the latter on surface stress overshadows the former, leading to a negative tendency in GW stress. This is not always the case however – some latitude bands see a mean increase in GW stress.
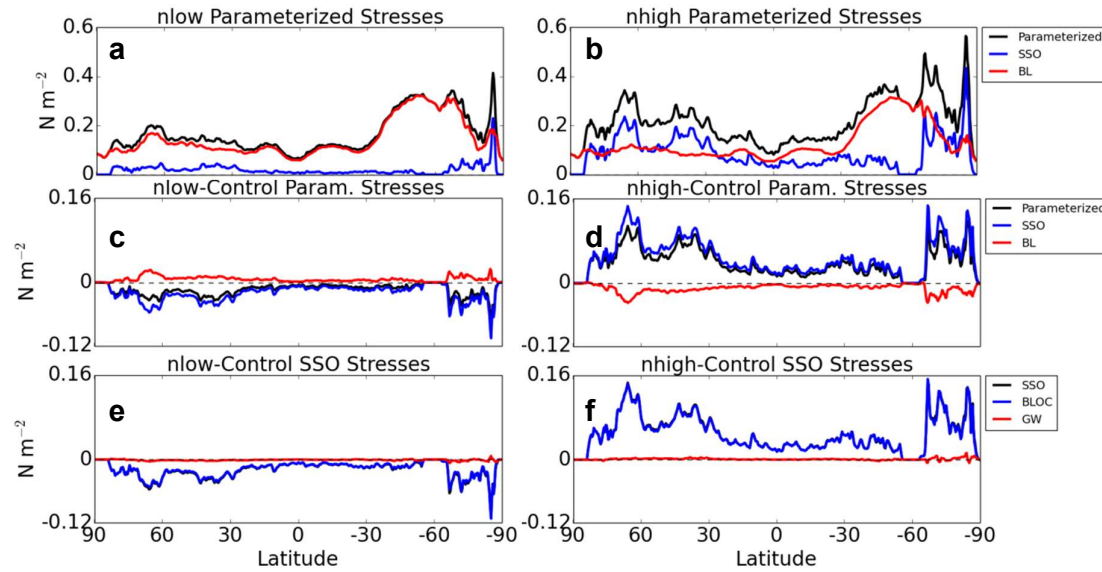

Figure 8. (a,b) Zonally averaged surface stress magnitudes and (c-f) stress magnitude differences relative to the *Control* experiment, averaged over the NWP integration using the *low* (left column) and *high* (right column) n_σ settings at a lead time of 24 hours.

The dramatic impact on stress representation due to n_σ changes is reflected in considerable changes in NWP and climate performance. A known shortcoming of the current operational global MetUM is a tendency to transport excess mass poleward, resulting in significant positive pressure biases over the polar ocean. This bias develops with forecast lead time, so is most apparent in climate simulations and the longer NWP ranges. It is clearly evident in mean sea level pressure (MSLP) and 500 hPa geopotential height in the *low* n_σ climate integration, as presented for MSLP in Figure 10a. This bias is largely eradicated and in places reversed in the *low* n_σ experiment; the decrease in surface stress leading to reduced meridional mass fluxes (Figure 10b,c). A corresponding increase in MSLP in lower latitudes further improves the picture, with reduced negative biases over South America and Africa in particular. Accordingly, area-weighted root mean square (RMS) errors (using ECMWF ERA-Interim reanalysis as "truth") in MSLP are reduced by 18 % during the NH winter. Note that, due to model instability using GA7.0, GA6.0 was employed for the *low* n_σ AMIP experiment (whilst all other experiments carried out for this study employ GA7.0).
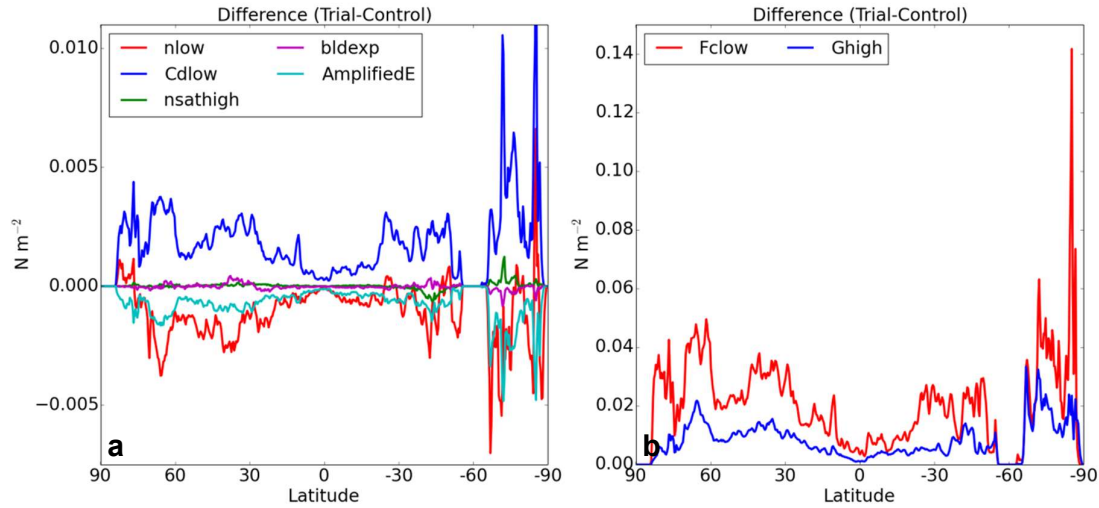
Figure 9. The impact of (a) *low n_σ* (red line), *low C_d* (blue), *high η_{sat}* (green), distributed TOFD (purple) and *amplified E(r)* (cyan); and (b) *low F_c* (red) and *high G* (blue) on zonally averaged GW stress magnitudes relative to the *Control* experiment at a lead time of 24 hours. Note difference in y-axis scales between the two panels.

A smaller improvement in MSLP is seen in the NWP integration (not shown); an improvement which is amplified with hindcast lead time as the polar pressure bias is given time to develop in the operational (*Control*) simulations. However, this improvement is tempered by worsening standard deviation errors; excessive variance in the mid to high NH latitudes indicating that the improvement is likely to some degree to be a product of compensating errors.
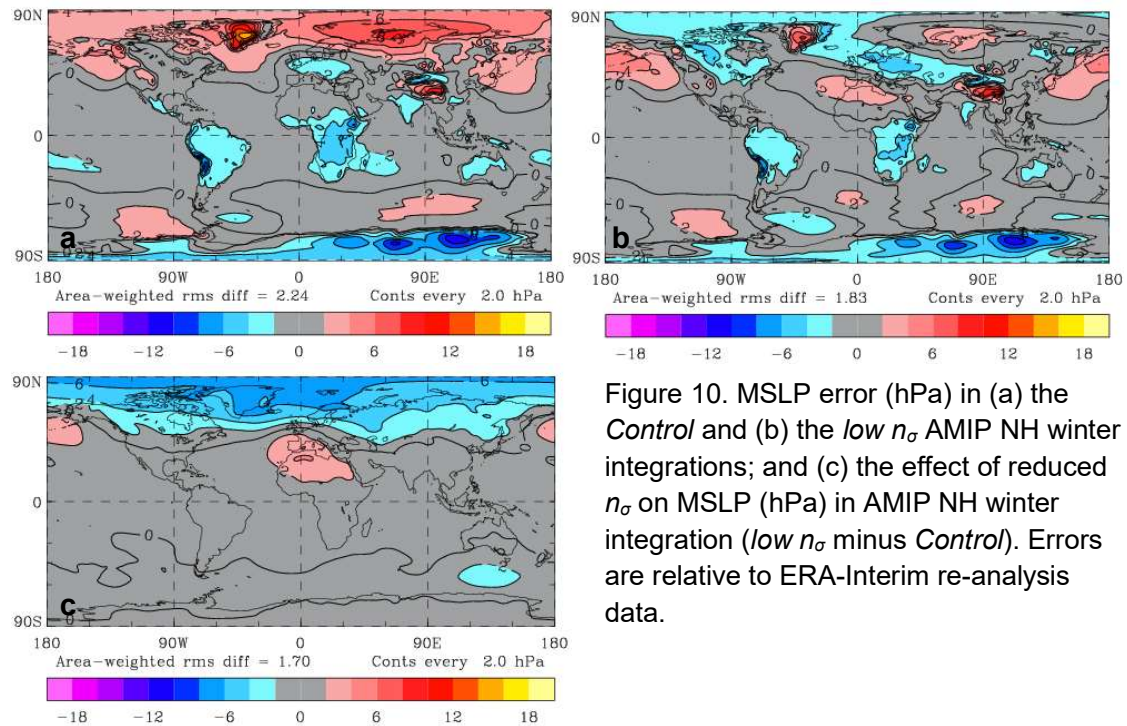

Figure 10. MSLP error (hPa) in (a) the *Control* and (b) the *low n_σ* AMIP NH winter integrations; and (c) the effect of reduced n_σ on MSLP (hPa) in AMIP NH winter integration (*low n_σ* minus *Control*). Errors are relative to ERA-Interim re-analysis data.

13

The improvement in MSLP is associated with a small improvement in 10 metre wind speeds in both NWP and climate integrations. In the NH during its winter this improvement is most apparent over North America, the North Atlantic and much of Russia (Figure 11a,b). A strong negative wind anomaly over the North Atlantic and the UK is largely eradicated (and in places reversed). The enhancement in wind speeds in this area is related to a strengthening of the mid-latitude westerlies (shown for the NWP integration in Figure 11c); a consequence of the reduction in BLOC stresses.
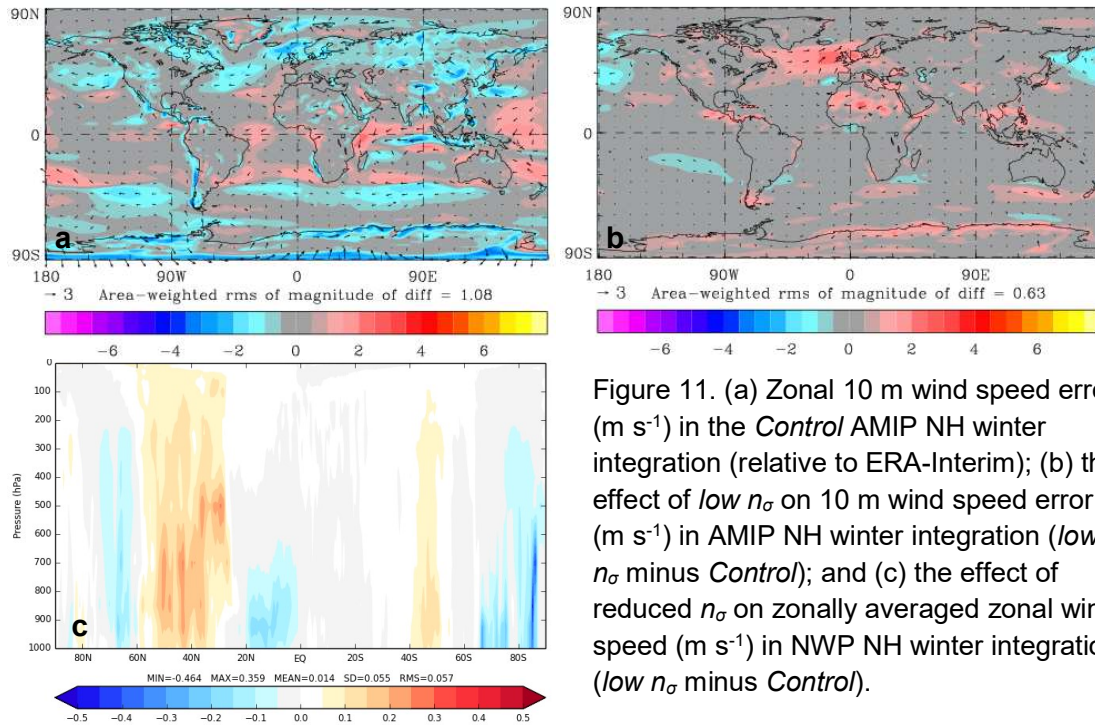

Figure 11. (a) Zonal 10 m wind speed error (m s^{-1}) in the *Control* AMIP NH winter integration (relative to ERA-Interim); (b) the effect of *low n_σ* on 10 m wind speed error (m s^{-1}) in AMIP NH winter integration (*low n_σ* minus *Control*); and (c) the effect of reduced n_σ on zonally averaged zonal wind speed (m s^{-1}) in NWP NH winter integration (*low n_σ* minus *Control*).

Unsurprisingly, the *high n_σ* experiment has disastrous effects on NWP and climate model performance (not shown), serving as it does to enhance the polar mass flux and thus exacerbate the pressure bias problem. On the other hand, in the upper atmosphere there are some minor improvements to upper level winds and temperatures, likely attributable to the increase in GW stresses (barely apparent in Figure 8f, though roughly equal in magnitude and opposite in sign to the effect of *low n_σ*, shown in Figure 9a). Such upper-level improvements are seen and discussed later on in other trials where GW stress is enhanced.

4.2.2 Flow blocking drag coefficient, C_d

This drag coefficient linearly modulates the parameterized flow blocking drag. It is set to a value of 4 in the operational global model, and has been shown to lie within the range 1 to 5 (from calculations based on results shown in Vosper et al., 2009). Here, experiments are run with C_d set to a *low* value of 0.5 and a *high* value of 8.

The impact on NH winter surface stresses to changes in C_d is generally similar to that to changes in n_σ. Changes in BLOC stress are, by definition, correlated with those in C_d, and partially balanced by a smaller, local compensating tendency in BL

stress (Figure 12). In the parameter settings trialled here, the impacts on BLOC and BL stresses are more acute than they are in the n_σ trials. A decrease in GW stresses provides an additional, smaller compensating response to the increase in BLOC (Figure 9). This GW stress tendency is the opposite of that seen in the n_σ experiments; a difference due to GW stress being a function of C_d only indirectly via wind speed and stability changes, but a direct (and generally inversely correlated) function of n_σ.
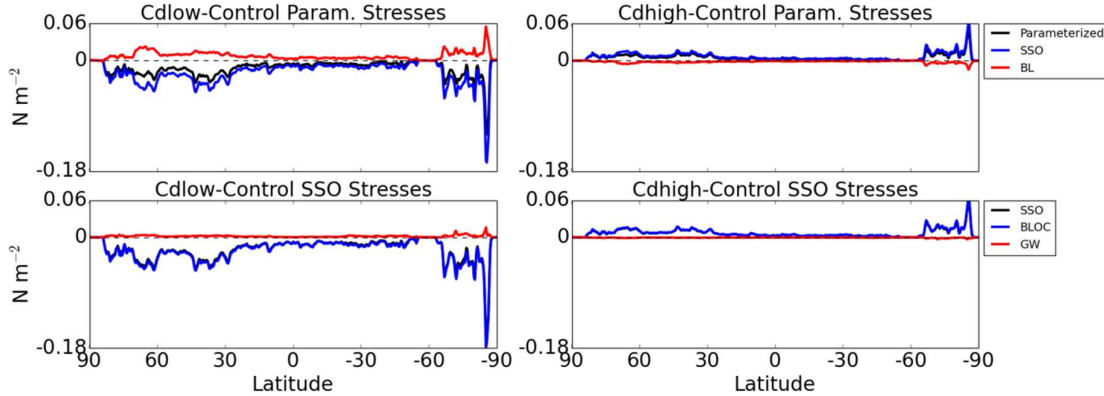

Figure 12. The impact of C_d alterations on zonally averaged surface stress magnitudes relative to the *Control* experiment, averaged over the NWP integration using the *low* (left column) and *high* (right column) C_d settings at a lead time of 24 hours.

As with n_σ, reducing C_d reduces polar mass fluxes and has a beneficial impact on MSLP, particularly in the climate integration (Figure 13) and to a lesser degree in the NWP integrations (not shown). Contrary to the *low n_σ* configuration, there is also marked improvement in MSLP over the Southern Hemispheric high latitudes; a low pressure bias over Antartica lifted likely as a result of increased incursion of flow over Antarctica due to the reduced flow blocking. Despite this, the global improvement in terms of RMS error in MSLP relative to ERA-Interim (14 % reduction) in the climate integration is not as great as in the *low n_σ* trial (18 % reduction), and whilst 500 hPa height biases are improved in the climate integration, they are marginally worse in the NWP integration. On the other hand, in contrast to the *low n_σ* trial, the improvement in MSLP in the NWP integration is not marred by increasing error in the variance, which in this case is unaffected.

In the *low C_d* NWP integration there are significant reductions in negative low level (1.5 m) temperature biases over orography (Figure 14), amounting to a 16 % reduction in RMS error globally relative to ERA-Interim. These regions of enhanced temperatures largely coincide with enhanced downward sensible heat fluxes, likely as a result of enhanced turbulent mixing due to the increased BL drag over orography (compensating for the deficit in BLOC drag). Note that a similar though weaker improvement (9 % reduction in RMS error) is seen in the *low n_σ* configuration.

The indirect effect on GW stresses brought about by changes in C_d leads, via vertical gravity wave momentum fluxes, to model performance impacts on higher levels in the atmosphere. In the *low C_d* experiment, the additional GW drag is associated with notable improvements in both tropospheric and stratospheric temperatures (the RMS error in zonally averaged temperatures reducing by 18 %; Figure 15) – particularly in

15

the lower stratosphere (200 hPa temperature RMS error reducing by 21 %; not shown) – and minor improvements in zonal wind speeds (not shown). Note that such improvements are absent in the *low n_σ* trial, supporting the notion that changes in GW drag are primarily responsible for these improvements. Furthermore, the pattern of the temperature and zonal wind speed changes closely resemble those expected to result from increases in GW drag according to previous studies on the impact of drag in global circulation models (Palmer et al., 1986; Stephenson, 1994; Robinson, 1997). This includes a warming of the polar stratosphere (reducing a notable negative temperature bias in the model; Figure 15) and an equator-ward shift in the mid-latitude and subtropical jets as a result of a reduction in eddy forcing of the zonal flow (Stephenson, 1994).
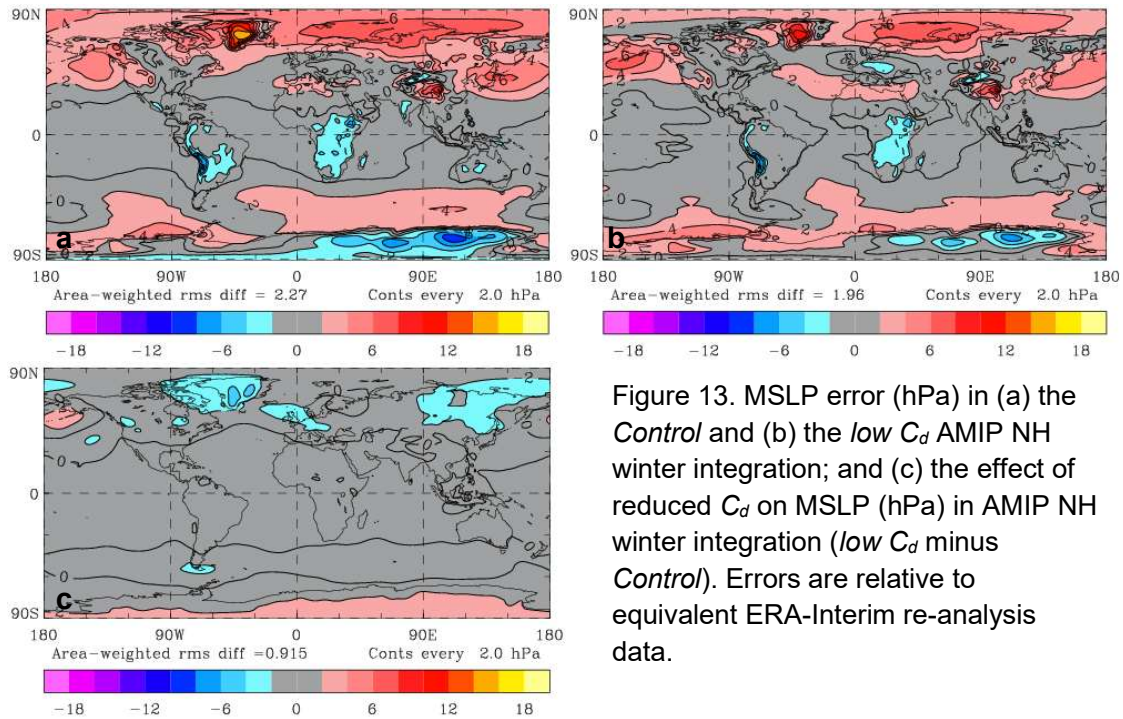

Figure 13. MSLP error (hPa) in (a) the *Control* and (b) the *low C_d* AMIP NH winter integration; and (c) the effect of reduced C_d on MSLP (hPa) in AMIP NH winter integration (*low C_d* minus *Control*). Errors are relative to equivalent ERA-Interim re-analysis data.
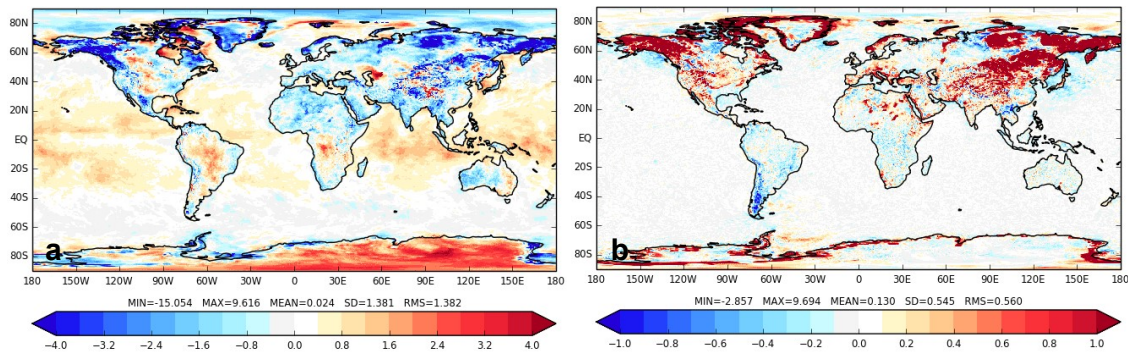

Figure 14. (a) Near-surface (1.5 m) temperature error (K) in the *Control* NWP NH winter integration (relative to equivalent ERA-Interim re-analysis data); (b) the effect of reduced C_d on 1.5 m temperature in the NWP NH winter integration (*low C_d* minus *Control*).
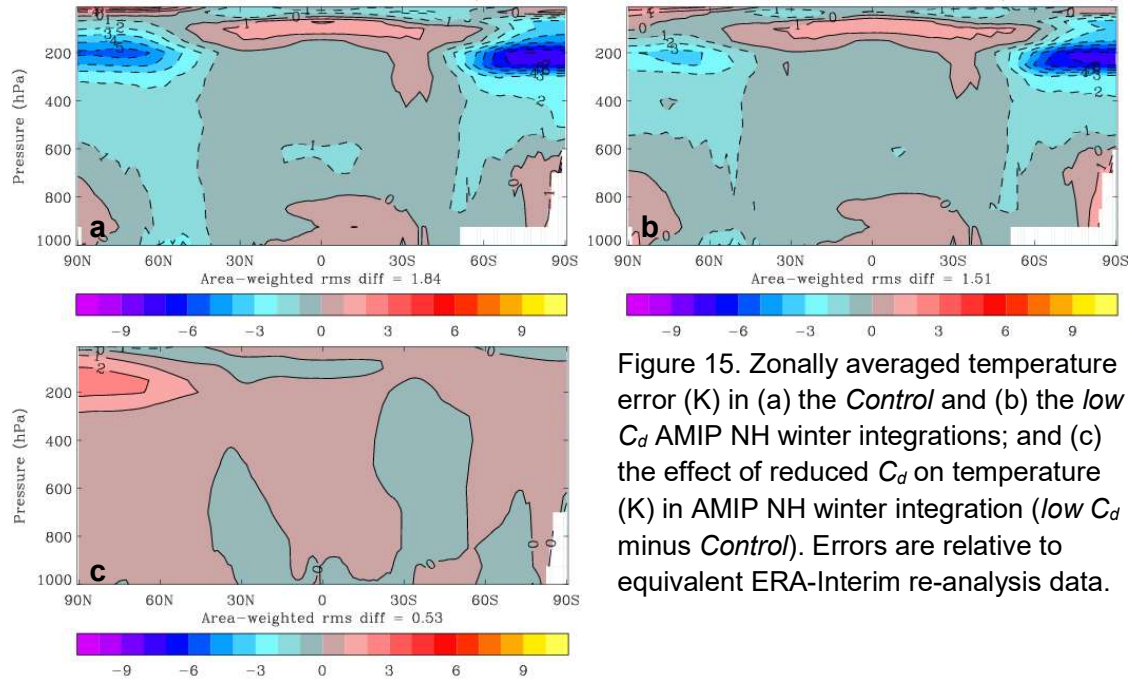
16

Figure 15. Zonally averaged temperature error (K) in (a) the *Control* and (b) the *low C_d* AMIP NH winter integrations; and (c) the effect of reduced C_d on temperature (K) in AMIP NH winter integration (*low C_d* minus *Control*). Errors are relative to equivalent ERA-Interim re-analysis data.

4.2.3 Critical Froude number, F_c

The critical Froude number determines the flow regime over the subgrid orography given the local depth-averaged Froude number and, consequently, the partition of parameterized drag between flow blocking and gravity wave breaking components. The value of this parameter is well constrained, using shallow water theory to a value of 1 (Durran, 1990) and linear theory in the range 0.7 to 1 (Smith, 1980). However, in the current operational global model this parameter is assigned the unphysical value of 4; such an elevated value should be expected to put an excessive proportion of the parameterized drag into low level flow blocking and not enough into higher-level gravity wave saturation. In the sensitivity tests a physically accurate value of 1 is trialled as well as an even higher value of 6.

The complex relationship between F_c and surface stresses is illustrated in Figure 16. In the *low F_c* trial, the impact on each of the SSO surface stress components is roughly equal and opposite, whilst in the *high F_c* trial, the comparatively small increase in BLOC dominates over the smaller-still decrease in GW. Interestingly, both trials generally yield an increase in total parameterized stresses, the reason for which is not obvious. The implication is that, given typical atmospheric conditions and the non-linear interactions between the various surface stress contributions and ensuing atmospheric conditions, the current operational value for F_c of 4 may yield the minimum in total surface stress as a function of F_c.
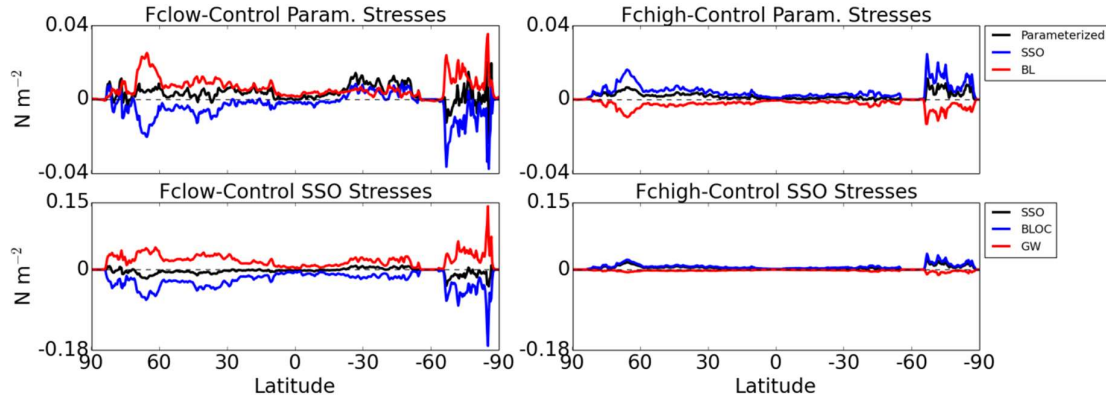
17

Figure 16. The impact of F_c alterations on zonally averaged surface stress magnitudes relative to the *Control* experiment, averaged over the NWP integration using the *low* (left column) and *high* (right column) F_c settings at a lead time of 24 hours.

As in the *low C_d* trial, the increase in GW drag caused by a decrease in F_c has favourable impacts on climate model performance in the upper atmosphere. The effect on GW momentum fluxes in the vertical in the *low F_c* trial is illustrated in Figure 17, from which it can be seen that the great majority of the additional GW stress is deposited to the mean flow beneath the 500 hPa height, particularly in the NH. As in the C_d trial, high latitude stratospheric warming and an equator-ward shift in the subtropical jet in both hemispheres are observed. Both these changes are beneficial to model performance in the climate integration; the former associated with a RMS error reduction in 200 hPa temperatures of 21 % (not shown) and the latter (apparent in streamfunction at 200 hPa; Figure 18) resulting in an improved reproduction of 200 hPa winds speeds relative to ERA-Interirm (5 % reduction in RMS error).

These trends are not, however, evident in the equivalent NWP integration, in which there is a general deterioration in model performance across most fields. However, as for *low C_d*, favourable near-surface warming over orography is evident (not shown), coinciding with the enhanced BL stresses. At lower levels in the climate integration, the *low F_c* experiment yields an increase in poleward mass flux, which exacerbates the polar high pressure bias at both surface level and 500 hPa height.
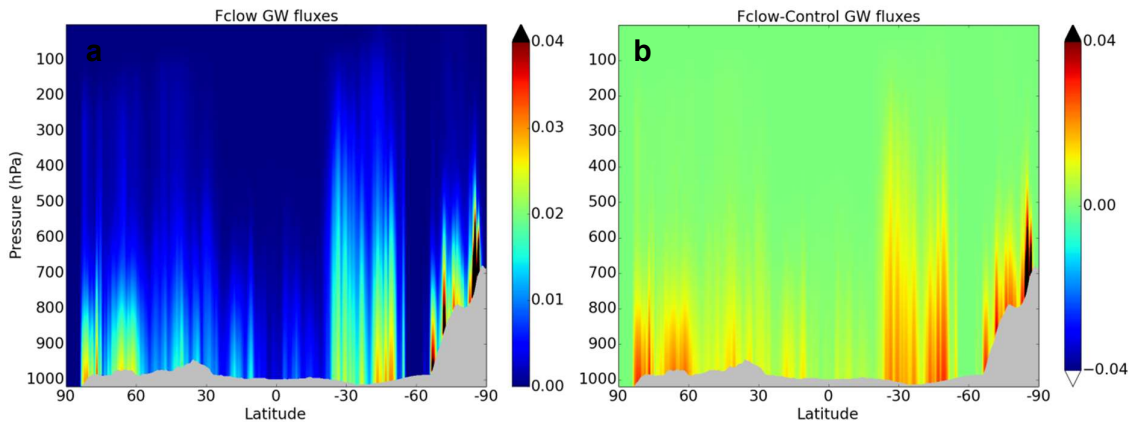

Figure 17. Vertical cross sections of (a) zonally-averaged orographic gravity wave stress (N m^{-2}), time-averaged over the *low F_c* NWP integration at a lead time of 24 hours and (b) the difference in this stress relative to that in the *Control* NWP integration (N m^2).
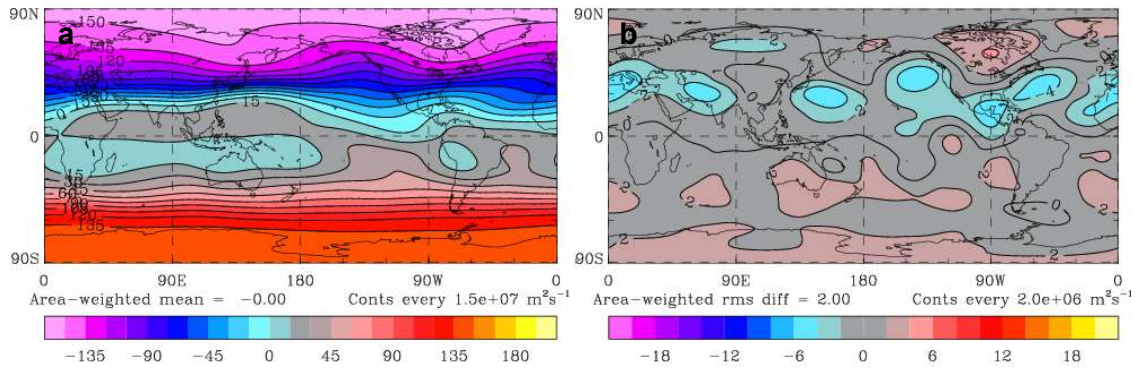
Figure 18. (a) Streamfunction (m^2 s^{-1}) at the 200 hPa height level from AMIP NH winter integration using operational (*Control*) settings. (b) Effect of reduced F_c on 200 hPa streamfunction (m^2 s^{-1}) from AMIP NH winter integration (*low C_d* minus *Control*).

4.2.4 Subgrid mountain sharpness, *G*

The mountain sharpness function, *G*, concerns the influence of the vertical cross-section of the barrier, i.e. the spacing of the elliptical terrain height contours, on the drag force (Phillips, 1984). It effectively modulates the amplitude of the parameterized vertically propagating gravity waves. Greater values of *G* describe a vertically "blunter" mountain, which results in a greater crosswind profile area, increasing the drag force exerted by the barrier via larger amplitude mountain waves. Phillips (1984) provides a typical range for *G* of 0.9 (for sharply peaked mountains) to 2 (for broad mountains). In the operational global model, *G* is outside of this range, set to a value of 0.5. Similar to the effect of the unphysically large operational value of F_c, this low value limits the gravity wave breaking contribution to orographic drag. New values of 0.1 and 1.5 are trialled here.

Owing to the fact that *G* only appears in the formulation of parameterized GW momentum flux and does not directly affect the generation or breaking of waves (and hence the spatial distribution of wave drag), the *G* trials afford direct assessment of the sensitivity of the MetUM to changes in GW stress magnitudes, just as that provided by the C_d for BLOC stresses. In the altered-*G* NWP integrations, impacts on BLOC and BL stresses are indirect and negligible (Figure 19), and the distribution of GW stresses are near-identical to those in the *Control* integrations (c.f. Figure 7).

The increase in GW stress brought about in the *high G* trial leads to similar consequences for stratospheric winds – strengthened (weakened) winds on the equator-ward (polar) flanks of the subtropical jet – and stratospheric temperature – warmer polar latitudes – as those in the C_d and F_c trials. In this case, whilst the improvement in model bias in stratospheric wind speeds is modest, the improvement in stratospheric (200 hPa) temperatures is substantial (Figure 20), with a 31 % reduction in bias relative to ERA-Interim. The impact of *high G* on low level conditions is for the most part negligible in the NWP integrations. There are however some detrimental effects in the climate integrations; most notably (as in the *low F_c* trial) an increase in the NH polar tropospheric high pressure bias.
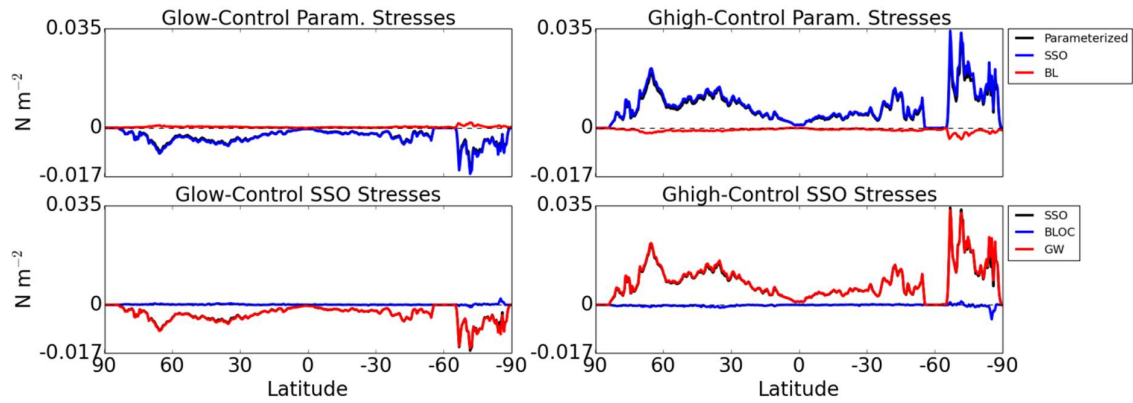
19

Figure 19. The impact of *G* alterations on zonally averaged surface stress magnitudes relative to the *Control* experiment, averaged over the NWP integration using the *low* (left column) and *high* (right column) *G* settings at a lead time of 24 hours.
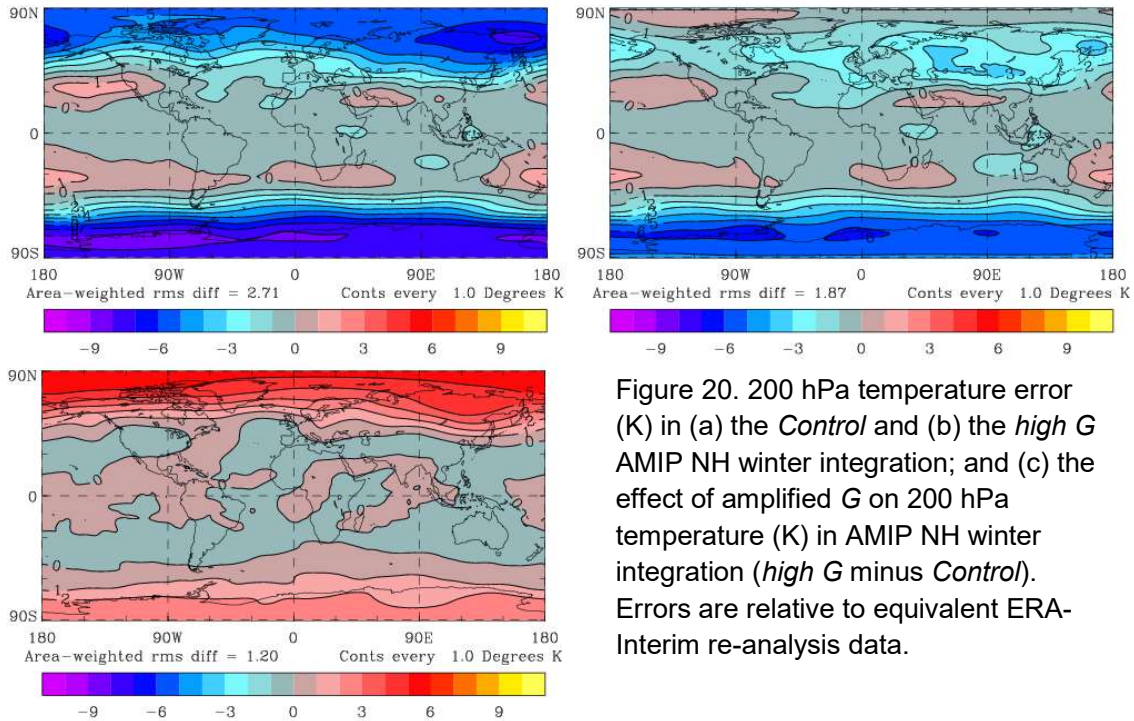

Figure 20. 200 hPa temperature error (K) in (a) the *Control* and (b) the *high G* AMIP NH winter integration; and (c) the effect of amplified *G* on 200 hPa temperature (K) in AMIP NH winter integration (*high G* minus *Control*). Errors are relative to equivalent ERA-Interim re-analysis data.

4.2.5 Critical non-dimensional wave amplitude, η_{sat}

Wave breaking is assumed to take place when the non-dimensional wave amplitude exceeds a critical value, η_{sat}. Consequently, the higher η_{sat} is, the higher in the atmosphere waves are able to propagate before breaking occurs and drag is exerted on the mean flow. In the operational global model, η_{sat} is set to 0.25, though its expected value lies in the range 0.5 to 2 (Webster et al., 2013). In the sensitivity experiments, *low* and *high* values of 0.2 and 2 are trialled.

The influence of η_{sat} on surface stresses is negligible since its only effect is to alter the height at which wave breaking occurs, as illustrated in Figure 21 for *high* η_{sat}. Here, the enhancement in GW stresses above surface level indicates an increase in

the height at which the drag is exerted on the mean flow. These stress enhancements are an order of magnitude smaller than those incurred in the *low F_c* and *high G* trials, and the resultant impact on NWP an climate integrations are limited. However, in the *high η_{sat}* NWP integration, there are minor reductions in RMS and standard deviation errors in many fields, in particular zonally averaged geopotential height, wind speeds and temperature, associated with reduced poleward mass fluxes at all altitudes. In climate integrations, however, both *low* and *high η_{sat}* generally have weakly detrimental effects on low level fields. Higher up in the atmosphere the *high η_{sat}* climate integration has a similar though smaller impact on temperature and winds as described in the enhanced GW stress cases of *low C_d*, *low F_c* and *high G*.
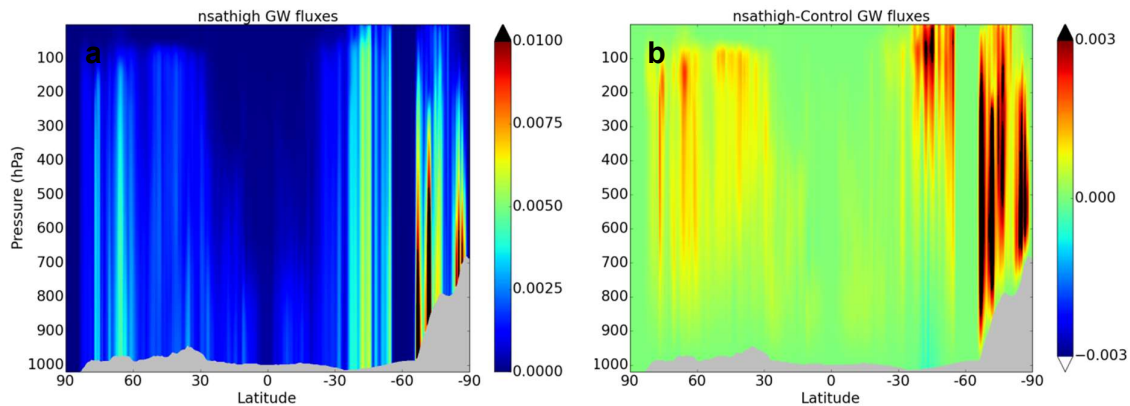

Figure 21. Vertical cross sections of (a) zonally-averaged orographic gravity wave stress (N m^{-2}), time-averaged over the *high η_{sat}* NWP integration at a lead time of 24 hours and (b) the difference in this stress relative to that in the *Control* NWP integration (N m^{-2}).

4.2.6 Distributed orographic form drag

An alternative representation of turbulent orographic form drag (TOFD) due to sub-grid hills is the explicit orographic stress parametrization proposed by Wood et al. (2001). In this case the drag is represented via an orographic stress term applied directly to the horizontal momentum equations as an additional explicit (in terms of time discretisation) stress. This scheme is trialled in replacement of the effective roughness approach.

Changes in zonally-averaged stresses due to the employment of the TOFD scheme are two orders of magnitude smaller than those incurred in the n_σ, C_d and F_c trials; the three parameters with the greatest impact on BL stress (Figure 22). For all three parameterized stress components the sign of the change varies with latitude, with the direct changes to BL partially compensated by changes in the SSO components and the greatest changes occurring in the more mountainous latitude bands (with peaks corresponding to the mountains of the Himalayas and the Rockies at ~40 °N and Antarctic orography at high southern latitudes). However, model sensitivities to the new scheme are generally negligible and not easily linked to the small and spatially variable changes in stress depicted in Figure 22.
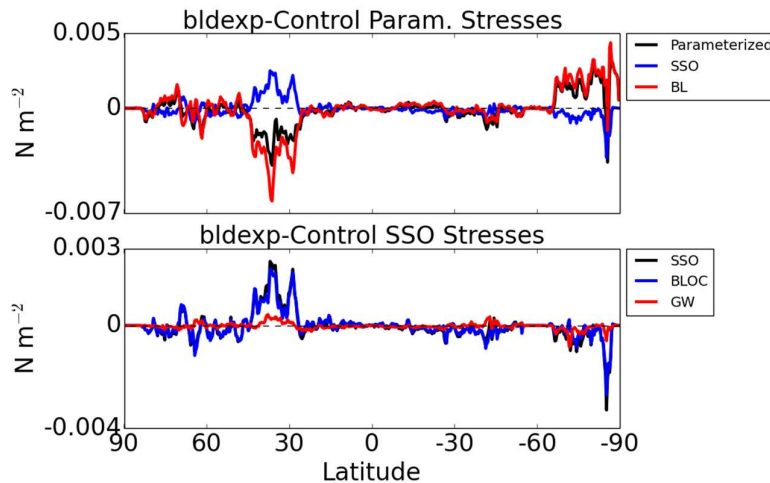
Figure 22. The impact of the new TOFD drag scheme on zonally averaged surface stress magnitudes relative to the *Control* experiment, averaged over the NWP integration at a lead time of 24 hours.

4.2.7 Aspect ratio dependent non-linear drag enhancement function, *E(r)*

The drag exerted on the atmosphere when air encounters a mountain is dependent on the mountain's aspect ratio as seen by the approaching flow. When the flow is perpendicular to a long ridge, nonlinear processes such as vortex-shedding and low-level wave breaking enhances the drag. Wells et al. (2008) showed that such processes could amplify drag by between 50 and 70 % above the linear value across the island of South Georgia. To account for this enhancement, Lott and Miller (1997) recommended the linear drag be multiplied by the function *E(r)*, where *r* is the subgrid mountain aspect ratio. However, Vosper (2015) found that the function generally under-represents the dependence of parameterized drag on *r* as its derivation neglected the self-limiting interdependent relationship between drag and wind speeds. Consequently Vosper (2015) recommended an alternative form for *E*, with greater dependence on *r*: $E(r) = \max(5 - 1/r^3, 0)$ replacing $E(r) = \max(2 - 1/r, 0)$. This revised version – trialled here as *Amplified E(r)* – was found to produce an increase in the drag (by a factor greater than 2.5) for wind directions close to perpendicular to the ridge.

Due to its dependent on the shape of orography and wind direction (via *r*), the increase in BLOC stress brought about by *amplified E(r)* is spatially variable. These increases are partially compensated by decreases in GW and BL stresses (Figures 23 and 9). The impact of *amplified E(r)* on NWP is generally detrimental, with increased excess high latitude pressures likely linked to the increase in BLOC stresses, and stronger biases in low level winds and temperatures. These trends are largely consistent with the climate integration, though there some minor positive effects, in particular on upper level temperatures with a warming of the high latitudes – an effect which is difficult to reconcile with the stress tendencies.
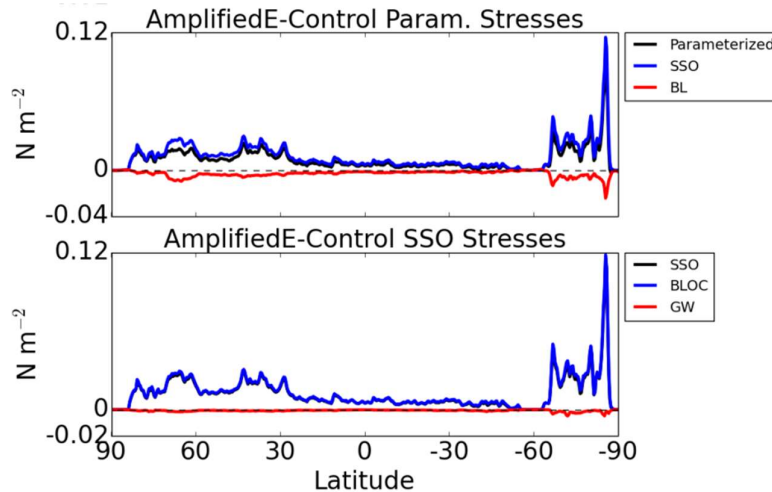
22

Figure 23. The impact of the *Amplified E(r)* on zonally averaged surface stress magnitudes relative to the *Control* experiment, averaged over the NWP integration at a lead time of 24 hours.

4.3 Summary

Tables 1 and 2 provide summaries of the sensitivity experiments, the latter presenting statistics based on the surface stress tendencies of each trial. Both SSO stress components are significantly affected in many of the trials. Whilst the absolute changes are on the whole considerably greater for BLOC stresses than for GW stresses, GW surface stresses are generally dwarfed by BLOC stresses and the percentage changes are comparable (Table 2). As previously mentioned, the two components influence the general circulation in very different ways, so comparison of their surface magnitudes is not pertinent. The BL stress component is generally more weakly and indirectly altered (only in the employment of the distributed TOFD scheme is it directly affected).

Generally, the configuration changes which yield the most beneficial changes to NWP and climate integrations are those which bring about a decrease in BLOC stresses and an increase in GW stresses. The former is brought about by decreasing n_σ, C_d or F_c, whilst the latter is caused by decreasing C_d (indirectly) or F_c, or by increasing G or n_σ. Furthermore, although barely affecting surface stress values, the impact of increasing η_{sat} has similarities to that of an increase in GW surface stress insomuch as the resulting redistributing of GW drag (wave breaking at higher levels) brings about an increase in drag in the upper atmosphere. The greatest change in GW stress comes from changes to one of the most reliably constrained drag parameters; F_c. Currently set to 4.0 operationally, F_c is known in reality to be about 1.0. Setting F_c to 1.0 in the MetUM results in a near-500 % increase in gravity wave drag and beneficial effects in the upper atmosphere where much of the gravity wave drag is felt.

It is important to note that changes which are beneficial to current operational model performance do not necessarily translate to improved parameterization; the challenge of which is to improve model performance for the right reasons, as opposed to compensating errors with others errors. Happily, for the majority of configuration changes here, model performance enhancements coincide with theoretically desirable changes in parameterization. For the three (of five) SSO parameters whose operational values fall outside their physically recommended ranges (F_c, G, η_{sat}), generally positive impacts on model performance are seen with

the parameter-changes to values within their physical ranges, whilst deteriorating model performance is seen with the changes in the opposite direction. The remaining two parameters, n_σ and C_d, currently fall within their physical range. However, the former is difficult to constrain and so there is some flexibility in its assignment, whilst the latter is currently set towards the upper end of its physically realistic range, and some key model performance improvements come about when it is reduced to a low 'extreme' beyond the low-end of this range (via decreased BLOC and increased GW stresses).

Of the two final configuration changes – employing the distributed TODF scheme and amplifying BLOC drag via the function $E(r)$ – the former has a largely insignificant effect on both the representation of drag and on model performance. The latter causes an increase in BLOC and decrease in GW stresses, resulting in a stronger and largely detrimental influence on both NWP and climate integrations.

One of the key effects of decreasing low level drag via BLOC stress on global circulation is to reduce the poleward mass flux, resulting in reduced high latitude pressures. This helps to reduce high pressure polar biases in the model, which extends throughout the depth of the atmosphere. A knock-on effect of reducing the BLOC stress is a compensating increase in BL stress. This has been demonstrated to have a beneficial effect on near-surface temperatures in all three trials in which BL stresses have increased (*low n_σ*, *low C_d*, *low F_c*), likely due to increased turbulent mixing in the boundary layer. The effect of enhanced GW drag in the upper atmosphere at climate time-scales is a warming of the high latitudes in the stratosphere and an equator-ward shift the mid-latitude and sub-tropical jets. The former leads to an often marked reduction in a substantial cool polar stratosphere bias that appears with operational settings, whilst the former generally results in marginal improvements in the representation of stratospheric circulation.

24

Parameter / config.	*Control* value	Physical range	Trial value	Effect on parameterized stresses					Key impacts of the more beneficial trial
				Total	BL	SSO	Bloc	GW	
n_σ	2.50 (=)	2.0 - 5.0 *	1.5	▽	(▲)	▼	▼	▽	*Low n_σ:* Weaker poleward mass transfer, stronger mid-lat. westerlies, increased excess NWP variances
			5	▲	(▼)	▲	▲	▲	
C_d	4.00 (=)	1.0 - 5.0 Vosper et al. (2009)	0.5	▽	(▲)	▼	▼	(▲)	*Low C_d:* Weaker poleward mass transfer, improved 1.5 m temperatures, high latitude stratospheric warming
			8	▲	(▼)	▲	▲	(▼)	
F_c	4.00 (▲)	0.7 - 1.0 Smith (1980)	1	▲	(▲)	▽	▼	▲	*Low Fc:* high latitude stratospheric warming and jet shift, generally detrimental to NWP, stronger poleward mass flux
			6	▲	(▼)	▲	▲	▼	
G	0.50 (▼)	0.9 - 2.0 Phillips (1984)	0.1	▽	(−)	▼	(−)	▼	*High G:* high latitude stratospheric warming and jet shift, stronger poleward mass flux
			1.5	▲	(−)	▲	(−)	▲	
η_{sat}	0.25 (▼)	0.5 - 2.0 Webster et al. (2013)	0.2	(−)	(−)	(−)	(−)	(−)	*High η_{sat}:* general minor improvements in NWP, generally detrimental to low-level climate
			2	(−)	(−)	(−)	(−)	(−)	
Distributed TOFD	–	–	–	–	–	(−)	(−)	(−)	Generally negligible impact
Amplified E(r)	–	–	–	▲	(▼)	▲	▲	▼	Generally detrimental to NWP and low level climate, marginally improved upper level temperatures

*The relatively poorly constrained stated physical range for n_σ is based on Lott and Miller (1997), who recommended a value of 2.0, and high resolution model studies of two mountain regions – South Georgia (Vosper, 2015) and New Zealand (Vosper et al., 2016) – for which values of 5.0 and 2.5 respectively were found to be appropriate.

Table 1: Summary of sensitivity experiments. *Control* value refers to the operational model parameter value, where '=', '▲' and '▼' refer to a value that is, respectively, within, above and below the physical range as recommended in the literature. In the "Effect on parameterized stresses" column: '▲' = positive tendency; '▼' = negative tendency; '–' = <1 % change; grey shading indicates a spatially variable change, where over 20 % of grid points exhibit the opposite tendency to that of the global average; brackets indicate a tendency that is an indirect effect of the configuration change. In the final column, green (red) text indicates an impact which is beneficial (detrimental) to model performance.

	Trial	low n_σ	low C_d	low F_c	high G	high η_{sat}	Dist. TOFD	Amplified $E(r)$
Param.	% diff.	-8	-7	2	4	0	0	5
	% -ive	45	47	51	56	56	57	54
	% +ive	55	53	49	44	44	43	46
BL	% diff.	5	5	5	-1	0	0	-2
	% -ive	66	64	57	34	57	59	36
	% +ive	34	36	43	66	43	41	64
SSO	% diff.	-51	-52	-8	20	0	0	31
	% -ive	0	3	26	99	52	39	97
	% +ive	100	97	74	1	48	61	3
BLOC	% diff.	-54	-63	-66	-1	0	0	36
	% -ive	0	0	0	47	49	39	100
	% +ive	100	100	100	53	51	61	0
GW	% diff.	-25	45	497	197	0	-1	-18
	% -ive	23	90	97	100	57	40	10
	% +ive	77	10	3	0	43	60	90
Res.	% diff.	-7×10^{-4}	-2×10^{-3}	-2×10^{-3}	-8×10^{-4}	1×10^{-4}	-9×10^{-4}	2×10^{-3}
	% -ive	61	50	37	41	58	35	56
	% +ive	39	50	63	59	42	65	44

Table 2. Surface stress magnitude tendency statistics. "% diff." refers to the global-mean tendency of each surface stress component as a percentage of the global-mean magnitude of that stress in the operational (*Control*) experiment. "% -ive" and "% +ive' are the percentage of grid boxes globally for which the tendency is positive and negative respectively. White text highlights where the tendency is <1 % (corresponding with the dashes in the "Effect on parameterized stresses" column of Table 1), and grey shading indicates a spatially variable change, where over 20 % of grid points exhibit the opposite tendency to that of the global average (corresponding with the grey shading in Table 1). Note that the resolved ('Res.') stresses are output directly from the model as the product of the resolved terrain slope and the pressure in each grid box.

5   Conclusions

A month-long comparison of surface stresses between the MetUM and ECMWF IFS reveals considerable differences in the representation of orographic drag, despite employing parameterizations based on the same scheme. In particular, the MetUM partitions a great deal more of its drag into flow blocking, whilst in the IFS boundary layer drag is much greater. This results in differences in spatial and diurnal variability in surface stress between the two models. The marked inter-model differences highlight the considerable uncertainty which remains in the representation of orographic drag. Motivated by this fact, MetUM sensitivity experiments have been used to investigate the impact of one-at-a-time changes in orographic drag parameterization on MetUM performance. Via modifications to the three components of parameterized orographic drag – flow blocking, gravity wave drag and turbulent form drag – major changes in the simulation of weather and climate are observed in both NWP and AMIP-style climate integrations. In many cases, these changes are favourable with respect to model performance. Such favourable changes tend to be associated with a decrease in flow blocking drag and/or an increase in GW drag. The

former helps to address one of the major deficiencies in the current operational MetUM – excessive transport of mass to the high latitudes – which results in a positive north polar and Southern Ocean pressure bias. The 'beneficial' combination of decreased flow blocking and increased BL drag in the MetUM brings the MetUM and IFS closer to agreement in the partition of orographic drag.

Recent attention at the Met Office has been given to the potential for model performance improvement by decreasing the subgrid mountain height parameter, n_σ. In this study, however, several of the other parameters have been found to provide similar benefits. In particular, a decrease in the flow blocking drag parameter, C_d, results in many of the beneficial outcomes of decreased n_σ such as reduced positive polar pressure biases (linked to decreases in flow blocking drag) and improved near surface temperatures (linked to enhanced boundary layer stress), though with additional benefits in the upper atmosphere such as polar stratospheric warming and an equator-ward shift in the mid latitude and sub tropical jets (linked to increases in gravity wave stress). Reductions in the critical Froude Number, F_c, and a mountain sharpness parameter, G, provide similar upper-level benefits. Further general improvements are seen by increasing the non-dimensional wave saturation amplitude, η_{sat}, whilst transition to a new turbulence form drag scheme produces more subtle effects.

The sensitivity experiments involve varying parameters between extremes, usually within their physically realistic ranges (as provided in the literature). Reassuringly, the signs of each of the beneficial parameter changes listed above correspond for the most part to those required to bring each parameter within – or closer to the midpoint of – their physical ranges. Note that the exception is for n_σ; however the physical range of this parameter is poorly constrained, affording flexibility in its allocation. To arrive at an "optimal" drag configuration which balances model performance with physically realistic parameter settings, it is likely that a combination of parameter changes will be necessary. Consequently, further sensitivity testing is recommended based on the findings of this study in which more than one parameter is altered at a time. In these tests, in addition to incorporating parameter changes it is recommended that the new, more sophisticated, distributed orographic form drag scheme be incorporated, as well as the theoretically preferable amplified form of the aspect ratio dependent non-linear drag enhancement function, $E(r)$. The latter's generally negative impact on model performance in the one-at-a-time sensitivity tests revealed here will not necessarily be pertinent in experiments where more than one parameter is changed at a time. Finally, an additional configuration change not investigated in this study should also be incorporated. This adaption involves additional filtering in the generation of subgrid orography fields to account for scales longer than the grid length (up to the "effective resolution" of orographic features).

In the inter-model comparison, the variability in drag partition gave rise to differences in diurnal and spatial variability in surface stresses, with the MetUM reproducing marginally larger-amplitude diurnal variability in all three drag components. Further investigation into such diurnal variability could be fruitful. For example, observations or high resolution modelling over mountainous regions could be used to gauge the real-world diurnal signature in drag, and consequently to provide insight into the correct partition between the subgrid orographic drag components and the turbulent

boundary layer drag (bearing in mind that the two have opposite-sign tendencies to changes in static stability).

Acknowledgements

References

Beljaars, A., Brown, A. R., & Wood, N. (2004). A new parametrization of turbulent orographic form drag. *Quarterly Journal of the Royal Meteorological Society*, *130*(599), 1327-1347.

Chen, G., Held, I. M., & Robinson, W. A. (2015). Sensitivity of the latitude of the surface westerlies to surface friction. *Journal of the atmospheric sciences*, *72*(9). Durran, D. R. (1990). Mountain waves and downslope winds. *Meteor. Monogr*, *23*, 59-81.

ECMWF (2013). IFS Documentation - Cy41r2. Part IV: Physical Processes, http://www.ecmwf.int/sites/default/files/elibrary/2016/16648-part-iv-physical-processes.pdf

Holton, J. R., & Hakim, G. J. (2012). *An introduction to dynamic meteorology* (Vol. 88). Academic press.

Lott, F., & Miller, M. J. (1997). A new subgrid-scale orographic drag parametrization: Its formulation and testing. *Quarterly Journal of the Royal Meteorological Society*, *123*(537), 101-127.

Mason, P. J. (1987). Diurnal variations in flow over a succession of ridges and valleys. *Quarterly Journal of the Royal Meteorological Society*, *113*(478), 1117-1140.

McFarlane, N. A. (1987). The effect of orographically excited gravity wave drag on the general circulation of the lower stratosphere and troposphere.*Journal of the atmospheric sciences*, *44*(14), 1775-1800.

Palmer, T. N., Shutts, G. J., & Swinbank, R. (1986). Alleviation of a systematic westerly bias in general circulation and numerical weather prediction models through an orographic gravity wave drag parametrization.*Quarterly Journal of the Royal Meteorological Society*, *112*(474), 1001-1039.

Phillips, D. S. (1984). Analytical surface pressure and drag for linear hydrostatic flow over three-dimensional elliptical mountains. *Journal of the atmospheric sciences*, *41*(6), 1073-1084.
Pithan, F., Angevine, W., & Mauritsen, T. (2015). Improving a global model from the boundary layer: Total turbulent energy and the neutral limit Prandtl number. *Journal of Advances in Modeling Earth Systems*, *7*(2), 791-805.

Robinson, W. A. (1997). Dissipation dependence of the jet latitude. *Journal of climate*, *10*(2), 176-182.

Sandu, I., Beljaars, A., Bechtold, P., Mauritsen, T., & Balsamo, G. (2013). Why is it so difficult to represent stably stratified conditions in numerical weather prediction (NWP) models?. *Journal of Advances in Modeling Earth Systems*, *5*(2), 117-133.

Sandu, I., Bechtold, P., Beljaars, A., Bozzo, A., Pithan, F., Shepherd, T. G., & Zadra, A. (2016). Impacts of parameterized orographic drag on the Northern Hemisphere winter circulation. *Journal of Advances in Modeling Earth Systems*.

Scinocca, J. F., & McFarlane, N. A. (2000). The parametrization of drag induced by stratified flow over anisotropic orography. *Quarterly Journal of the Royal Meteorological Society*, *126*(568), 2353-2393.

Smith, R. B. (1980). Linear theory of stratified hydrostatic flow past an isolated mountain. *Tellus*, *32*(4), 348-364.

Stephenson, D. B. (1994). The Northern Hemisphere tropospheric response to changes in the gravity-wave drag scheme in a perpetual January GCM. *Quarterly Journal of the Royal Meteorological Society*, *120*(517), 699-712.

Vosper, S. B., Wells, H., & Brown, A. R. (2009). Accounting for non-uniform static stability in orographic drag parametrization. *Quarterly Journal of the Royal Meteorological Society*, *135*(640), 815-822.

Vosper, S. B. (2015). Mountain waves and wakes generated by South Georgia: implications for drag parametrization. *Quarterly Journal of the Royal Meteorological Society*, *141*(692), 2813-2827.

Vosper, S. B., Brown, A. R., & Webster, S. (2016). Orographic drag on islands in the NWP mountain grey zone. *Quarterly Journal of the Royal Meteorological Society*.

Webster et al., 2013 Gravity Wave Drag, Unified Model Documentation Paper No. 22

Wood, N., & Mason, P. (1993). The pressure force induced by neutral, turbulent flow over hills. *Quarterly Journal of the Royal Meteorological Society*, *119*(514), 1233-1267.

Wood, N., Brown, A. R., & Hewer, F. E. (2001). Parametrizing the effects of orography on the boundary layer: An alternative to effective roughness lengths. *Quarterly Journal of the Royal Meteorological Society*, *127*(573), 759-777.

Zadra, A., Roch, M., Laroche, S., & Charron, M. (2003). The subgrid-scale orographic blocking parametrization of the GEM Model. *Atmosphere-ocean*,*41*(2), 155-170.

Zadra, A. (2015). *WGNE drag project: An inter-model comparison of surface stresses*. technical report [Available at http://collaboration. cmc. ec. gc. ca/science/rpn/drag_project/documents/wgne_drag_project_report01. pdf].